Vibrational structures of methylamine isotopomers in the predissociative $\tilde{A}$ states: CH_3NHD, CD_3NH_2, CD_3NHD, and CD_3ND_2

Min Hee Park, Kyo-Won Choi, Sunyoung Choi, and Sang Kyu Kim[a)]
Department of Chemistry and School of Molecular Sciences (BK21), Korea Advanced Institute of Science and Technology (KAIST), Daejeon 301-750, Korea

Young S. Choi[b)]
Department of Chemistry, Inha University, Incheon 402-751, Korea

(Received 15 June 2006; accepted 26 July 2006; published online 28 August 2006)

Mass-resolved two-photon (1+1) resonance-enhanced multiphoton ionization spectra of the $\tilde{A}$-X transitions of various methylamine isotopomers (CH_3NHD, CD_3NH_2, CD_3NHD, and CD_3ND_2) cooled in the supersonic jet expansion have been measured and analyzed. The band analysis using the Hamiltonian for the internal and overall rotational motions provides the accurate vibrational band positions, allowing for unambiguous assignments for all observed vibrational bands of methylamine isotopomers in the $\tilde{A}$ states. Amino wagging (ν_9) and methyl rocking (ν_7) modes are found to be Franck-Condon active, and associated anharmonicity constants are precisely determined to give the detailed shape of the potential energy surface in the vicinity of the minimum electronic molecular structure. The barrier height for the nearly free internal rotation about the C–N bond in the $\tilde{A}$ state is calculated to be strongly dependent on the excitation of the other higher-frequency vibrational modes, and it is found that the trend is consistent with the experiment. Experimentally measured spectroscopic constants are compared with *ab initio* calculations, confirming all vibronic assignments. Experimental and theoretical results on all possible H/D isotopomers of methylamine in this work, with the earlier report on CH_3NH_2 and CH_3ND_2 Baek *et al.*, [J. Chem. Phys. **118**, 11026 (2003)], provide the complete spectroscopic characterization of the $\tilde{A}$ state of methylamine. © *2006 American Institute of Physics*. [DOI: 10.1063/1.2338322]

I. INTRODUCTION

Methylamine (CH_3NH_2) is the simplest primary amine which constitutes amino acids and a variety of heterocyclic compounds. The structure and chemical reactivity of methylamine exposed to various external conditions are therefore quite essential for the understanding of many organic and/or biological reactions involving primary amines as reactants or products. Photochemistry of methylamine has long been investigated for unraveling the structure of the excited state and various reaction channels.[1–15] Even though many previous spectroscopic and dynamic works on methylamine had been reported in the mid-1990s[9–14] the proper spectroscopic characterization of the excited methylamine has only recently been established.[16–18] In our earlier report, rovibrational structures of CH_3NH_2 and CH_3ND_2 in the excited $\tilde{A}$ state have been investigated by using the resonance-enhanced (1+1) two-photon ionization (R2PI) spectroscopic method.[16–18] Due to the relatively long lifetimes of the excited states of CH_3ND_2 rotational fine structures could be well resolved for the first few vibronic bands to provide accurate spectroscopic constants associated with rovibrational motion of the excited CH_3ND_2 molecule.[16–18] The rather broad vibronic bands of the excited CH_3NH_2 have also been very successfully analyzed based on the internal/overall-rotational Hamiltonian used for the analysis of CH_3ND_2. According to the structural change from the NH_2 bent to NH_2 planar with respect to the C–N axis upon the electronic transition, NH_2 wagging and CH_3 rocking modes are found to be mostly active in the $\tilde{A}$-X transition, and their vibrational term values has been accurately determined. Vibronic band broadening is found to be due to the fast N–H(D) bond dissociation in the predissociative $\tilde{A}$ state.[16–18]

Therefore, it is now well known that methylamine, in its excited state, undergoes the N–H bond dissociation through the vibronic coupling of the optically bright n-3s Rydberg state to the dissociative valence electronic state. At the zero-point energy level the N–H dissociation proceeds via tunneling through a reaction barrier, showing the huge H/D isotope effect in the reaction rate.[16–18] Internal rotation of methylamine around the C–N axis becomes nearly free in the first electronically excited state, and the barrier height of 5 cm^{-1} at the zero-point energy level of the excited CH_3ND_2 has been accurately estimated from the spectroscopic analysis. Although our earlier report on methylamines in the $\tilde{A}$ state has provided these essential spectroscopic and dynamic features,[17,18] the exploration of other isotopomers are necessary for the complete spectroscopic characterization of methylamines in the electronically excited state. In this work, we investigate all other possible isotopomers of methy-

[a)]Electronic mail: sangkyukim@kaist.ac.kr
[b)]Electronic mail: yschoi@inha.ac.kr

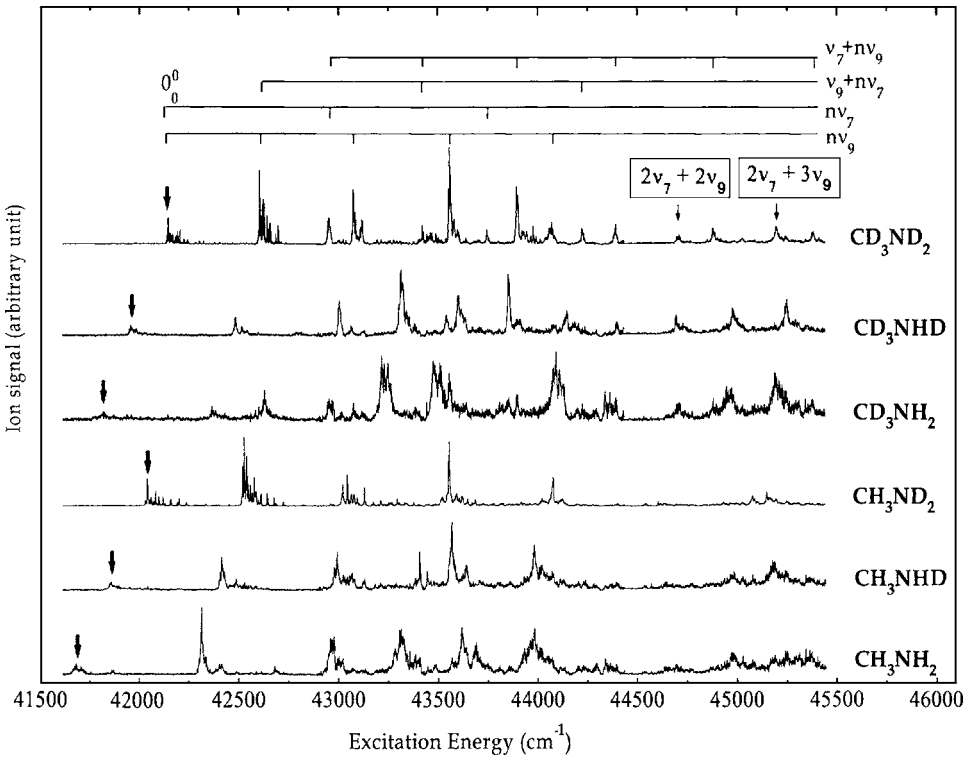

FIG. 1. R2PI excitation spectra of six methylamine isotopomers (CH_3NH_2, CH_3NHD, CH_3ND_2, CD_3NH_2, CD_3NHD, and CD_3ND_2) in the 41 600–45 550 cm^{-1} range. Arrows indicate the spectral origin positions.

lamines using the resonance-enhanced two-photon ionization spectroscopy to give associated spectroscopic constants. This work completes the spectroscopic characterization of methylamines in the $\tilde{A}$ state, providing the firm framework for future dynamics studies. *Ab initio* calculations at the complete active space self-consistent field (CASSCF) level with the 6-31++G(d,p) basis set are carried out for the excited $(\tilde{A})$ methylamines to be compared with the experiment.[19] In the earlier report, it has been found that the internal-rotor barrier height in the methylamine $\tilde{A}$ state increases with the vibrational excitation.[17] Theoretical interpretation for this experimental observation is also presented here.

II. EXPERIMENT

Various methylamine isotopomers were prepared by keeping the 1:1 mixture of CH_3NH_2 (Aldrich, 98%) and CD_3ND_2 (Cambridge Isotopes, 98%) gases in a lecture bottle for several days. The resultant sample mixture contained all possible methylamine isotopomers; CH_3NH_2, CH_3NHD, CH_3ND_2, CD_3NH_2, CD_3NHD, and CD_3ND_2 by the H/D exchange reactions. Methylamine isotopomers were introduced into a gas cylinder to be mixed with Ne with a concentration of ~1%. The gas mixture was then expanded into vacuum through a nozzle orifice (General Valve 9 Series) with a backing pressure of ~3.5 atm and a repetition rate of 10 Hz. The 355 nm output of a Nd:YAG (yttrium aluminum garnet) laser (Continuum, Precision II 8010) was used to pump a dye laser (Lumonics, HD500) to generate laser pulses in the 440–480 nm range. The absolute laser wavelength was calibrated within ±0.1 cm^{-1} by the use of a wavemeter (Coherent, 33-2619). The output of the dye laser was frequency doubled in a beta barium borate (BBO) crystal placed on a homemade autotracking system to generate the tunable laser pulse in the 220–240 nm range. The UV laser pulse was then overlapped with the molecular beam spatially and temporally to ionize methylamines by the (1+1) R2PI process. The ions were extracted, accelerated, drifted along the field-free region, and detected by microchannel plates (MCPs) (Jordan). The signal was digitized by an oscilloscope (LeCroy, LT584) and stored in a personal computer. *Ab initio* calculations were carried out by using the GAUSSIAN 03 program package using a personal computer.[19] The excited state geometry and fundamental vibrational frequencies were calculated using the complete active space self-consistent field [CASSCF(6,6)] method with a 6-31++G(d,p) basis set.

III. RESULTS AND DISCUSSION

The $\tilde{A}$-X excitation spectra of all six different methylamine isotopomers (CH_3NH_2, CH_3NHD, CH_3ND_2, CD_3NH_2, CD_3NHD, and CD_3ND_2) taken in the 41 660–45 550 cm^{-1} region are shown with appropriate assignments in Fig. 1. The major structural change of methylamine induced by the electronic transition ($3s$-n) is that the bent amino group becomes planar in the excited state. Accordingly, the NH_2 wagging mode (ν_9) is most active in the excitation spectrum giving a quite long progression. Another active mode is found to be the CH_3 rocking mode (ν_7), and the corresponding progression and combination modes are identified in all of excitation spectra in Fig. 1. It is found that the rotational structure of the origin and first ν_9 band is well resolved for CD_3ND_2 and CH_3ND_2, while it is not resolved for CH_3NHD, CD_3NHD, CH_3NH_2, and CD_3NH_2. This experimental finding confirms that the broadening of the vibronic bands of the $\tilde{A}$ state methylamine is originated from the ultrafast N–H bond predissociation, as has been reported

in Ref. 17. Only isotopomers with the ND_2 moiety, because of the much decreased tunneling rate of the N–D dissociation, show the narrow linewidths in the first few vibronic bands revealing the detailed spectroscopic constants associated with internal and overall rotations. The lifetime of the predissociative $\tilde{A}$ state of methylamine is found to be little changed by the H to D substitution on the methyl moiety. The partial H to D substitution on the amino group is not effective in reducing the linewidth of the vibronic band, indicating that the predissociation occurs exclusively along the N–H coordinate with a reaction barrier through which the tunneling rate leading to the N–D bond rupture is significantly slowed down due to the larger mass of D.

A. Spectral analysis for the excitation spectrum of CD_3ND_2 ($\tilde{A}$)

The band positions are precisely located by comparing the rotationally resolved peaks with the simulated ones based on the overall/internal rotor Hamiltonian with a small barrier along the torsional angle around the C–N axis. The detailed spectral analysis for CH_3NH_2 and CH_3ND_2 was already given previously in Ref. 17. Here, we will show the analysis for the rotationally resolved vibronic bands of the excited CD_3ND_2. Analyses of vibronic bands of CD_3NH_2, CH_3NHD, and CD_3NHD have been carried out in the similar way. As the rovibrational levels in $\tilde{A}$ state are predissociative, the Lorentzian function convoluted with the proper Gaussian-shaped instrumental function is used for the vibronic band simulation. The full description of the simulation procedure had been given in our earlier report.[17] Briefly, the Hamiltonian for the overall/internal rotation is given as follows:

$$H = H_{\mathrm{rot}} + F(p - P)^2 + V(\phi). \tag{1}$$

Here, H_{rot} is the rigid-rotor Hamiltonian based on the symmetric-top approximation reflecting the overall rotation of the excited methylamine. F is the effective rotational constant for the internal rotation of the top (CH_3) with respect to the frame (NH_2). V is the sixfold torsional potential with a form of $V(\phi)=(V_6/2)\,[1-\cos(6\phi)]$ where V_6 is the barrier height along the torsional angle ϕ. The $(p-\mathrm{P})$ term is the relative angular momentum of the top and frame. The 100×100 Hamiltonian matrix is constructed with a free rotor basis set, $|m\rangle=(2\pi)^{-1/2}\exp(-im\phi)$ to give nonvanishing matrix elements as follows;

$$\langle m|H|m\rangle = (A^T + A^E)m^2 + BJ(J+1) + (A^F - B)K'^2 - 2A^F mK' + (V_6/2), \tag{2}$$

$$\langle m|H|m \pm 6\rangle = -(V_6/4), \tag{3}$$

where A^T and A^F are rotational constants of the top and frame, respectively, while B is the overall rotational constant and K' is the angular momentum of methylamine in the excited state. The resultant Hamiltonian matrix is diagonalized to give energies and associated eigenstates.

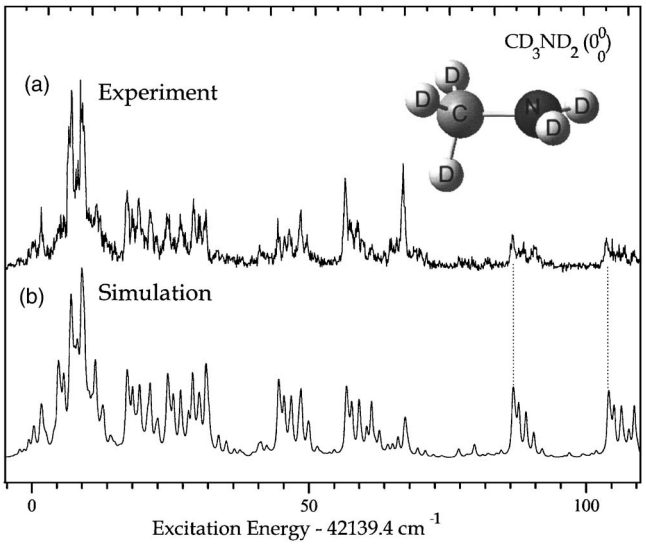

FIG. 2. (a) The origin band of CD_3ND_2 in the $\tilde{A}$-X transition shown with (b) the simulation based on the internal/overall rotational Hamiltonian (see the text for details).

In Fig. 2, the origin band of CD_3ND_2 is shown with the simulation with a $T_{\mathrm{rot}}=3.5$ K. Two sets of peaks denoted by dotted lines in Fig. 2 are very sensitive to the value of the torsional barrier height, giving $V_6=5.5\pm1.0$ cm^{-1} for the zero-point level of the $\tilde{A}$ state CD_3ND_2. This is quite similar to the torsional barrier height of 5.0 cm^{-1} which was found for CH_3ND_2 at the zero point level in Ref. 17. The torsional barrier of $CD_3ND_2(\tilde{A})$ is found to be 19 cm^{-1} when one quantum of the ν_9 mode is excited (Table I). The increase of the torsional barrier height with the ν_9 mode excitation has also been observed for CH_3ND_2.[17] The predissociation lifetime of the zero-point energy level of CD_3ND_2, extracted from the homogeneous linewidth of the spectrum is ~11 ps, and this is slightly larger than the lifetime of ~9 ps found for CH_3ND_2.[17] Thus except for rotational constants which are naturally changed by the H to D substitution, the underlying dynamics in terms of torsional motions and predissociation seem to remain nearly same even when the methyl group of CH_3ND_2 is totally deuterated to CD_3ND_2. Other vibronic bands are analyzed by the same procedure, and associated spectroscopic constants are listed in Table I. In this way, the positions of all the observed vibrational levels in the $\tilde{A}$ state of CD_3ND_2 could be quite accurately determined within the

TABLE I. Parameters used in the simulation for CD_3ND_2 excitation spectra. Parameters in parentheses are less reliable. $T_{\mathrm{rot}}=3.5$ K is used for all simulations.

	0_0^0	υ_9	υ_7	$2\upsilon_9$
A^T	4.95±0.1	4.56±0.1	(4.3)	(4.2)
A^F	2.50±0.1	2.47±0.1	(2.2)	(2.1)
B'	0.59±0.07	0.55±0.07	(0.5)	(0.5)
FWHM	0.50±0.03	0.50±0.03	(1.0)	(3.0)
τ (ps)	10.6±0.6	10.6±0.6	(5.3)	(1.8)
V_6	5.5±1.0	19±2	⋯	⋯
E_{vib}	0	456±1	799±1	932±1

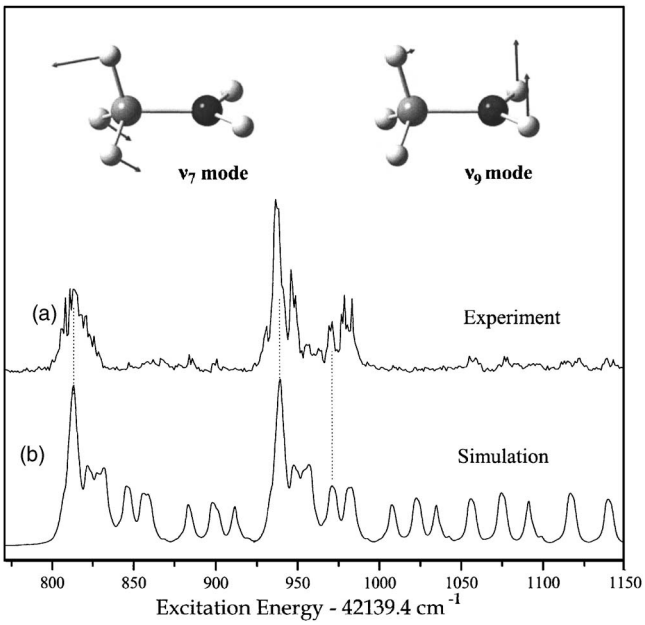

FIG. 3. (a) The R2PI spectrum of CD_3ND_2 for the ν_7 (CH_3 rock) and $2\nu_9$ (ND_2 wag) vibronic bands with (b) the simulation based on parameters listed in Table I. The normal mode description for ν_7 and ν_9 is given. The relatively poor simulation to the experiment in the high internal energy range is possibly due to vibronic couplings to optically dark states (see the text).

uncertainty of 2 cm^{-1}. In Fig. 3, vibronic bands corresponding to ν_7 and $2\nu_9$ modes of CD_3ND_2 ($\tilde{A}$) are compared with the simulation. It should be noted that the (ν_7, $2\nu_9$) modes were severely overlapped for CH_3ND_2,[17] and now those are clearly separated in the excitation spectrum of CD_3ND_2 to give the more accurate term values of two different modes. The overall shapes of the ν_7 and $2\nu_9$ bands are quite different from each other, suggesting that nuclear overlap integrals associated with internal rotational motion may be different for the two modes presumably because of the difference in the effective torsional potentials built on different vibrational excitations (*vide infra*). Both bands are quite broadened compared to the origin band due to the faster N–D predissociation, and precise determination of rotational constants is not trivial. Furthermore, detailed spectral features associated with internal rotations are relatively poorly reproduced by the simulation, suggesting that the anharmonic or Coriolis coupling to optically dark states might become important at high internal energies.

B. Vibrational term values and anharmonicity fitting

From the spectral analysis, the band origins of CH_3NH_2, CH_3NHD, CH_3ND_2, CD_3NH_2, CD_3NHD, and CD_3ND_2 are accurately located to be 41 664, 41 844, 42 035, 41 793, 41 948, and 42 139 cm^{-1}, respectively (Fig. 1). Thus it is quite secure to state that the long time confusion about the location of the origin band of the $\tilde{A}$-X transition for any methylamine isotopomer is now completely settled.[10–15] Band origins (T_o) of various isotopomers are listed in Table II. It should be noted that T_o is blueshifted with the H→D substitution. Very interestingly, the amount of T_o shift is found to be larger when the amino moiety is deuterated compared with that caused by the methyl group H/D substitution. This observation indicates that the N–H stretching mode in $\tilde{A}$ is more sensitive to the H→D substitution than the C–H stretching is. Time dependent density-functional theory (TD-DFT) calculation [B3LYP/6-31++G(d,p)] assuming the $\tilde{A}$ state geometry optimized by CASSCF [6-31++G(d,p)] gives T_e=41 598 cm^{-1}. Using this theoretical term value of T_e and vibrational frequencies calculated by CASSCF, T_o of each isotopomer is calculated to be compared with the experiment (Table II). Though absolute values are not exactly matched, the trend with the H/D substitution is quite consistent with the experiment. The anharmonicity especially along the predissociative N–H axis should be largely responsible for any mismatch between theory and experiment.

Term values for vibrational levels of each isotopomer in the $\tilde{A}$ state are obtained by subtracting the transition frequency of the origin band from the measured frequencies of vibronic bands. The measured vibrational term values of all isotopomers, which are given with respect to the zero-point levels, are summarized in Table III with appropriate assignments. The isotopic substitution provides the most conclusive clue to the proper mode assignment as the fundamental frequency of a particular mode shows a systematic shift upon isotopic substitution depending on the extent of involvement of the substituted nuclear motion in the corresponding normal mode. The frequencies of the amino-wagging mode are 636.4 cm^{-1} for CH_3NH_2, 546.5 cm^{-1} for CH_3NHD, and 482.6 cm^{-1} for CH_3ND_2. The fundamental frequencies and their isotopic shifts are in excellent agreement with the *ab initio* values calculated by the CASSCF(6,6) method with a 6-31++G(d,p) basis set (Table IV). The isotopic frequency

TABLE II. Experimental and theoretical band origins of various methylamine isotopomers (cm^{-1}).

	CH_3NH_2	CH_3NHD	CH_3ND_2	CD_3NH_2	CD_3NHD	CD_3ND_2
T_e[a]	41 598					
ZPE (X)	15 000	14 220	13 430	12 761	11 977	11 184
ZPE ($\tilde{A}$)[b]	13 893	13 207	12 519	11 685	11 017	10 338
T_o (Calc.)	40 490	40 584	40 686	40 521	40 637	40 752
T_o (Expt.)	41 664	41 844	42 035	41 793	41 948	42 139

[a]TD-DFT result calculated by the B3LYP method with a basis set of 6-31++G(d,p). T_o=T_e+ZPE($\tilde{A}$)−ZPE(X).

[b]ZPE for the torsional mode is not included since it is almost zero in the $\tilde{A}$ state.

TABLE III. Measured electronic origins and term values (cm^{-1}) for the vibrational levels of six methylamine isotopomers in the $\tilde{A}$ state. The numbers in parentheses are the differences between the measured values and fitted ones ($\nu_{obs}-\nu_{fit}$) (see the text for details).

Vibrational levels	Vibrational term values (cm^{-1})					
	CH_3NH_2	CH_3NHD	CH_3ND_2	CD_3NH_2	CD_3NHD	CD_3ND_2
0_0^0 [T_0]	0 [41664±1]	0 [41844±1]	0 [42035±1]	0 [41793±4]	0 [41948±2]	0 [42139±1]
ν_9	634(−2.4)	552(5.4)	480(0.7)	549(−11.3)	518(1.7)	456(−3.1)
ν_7	1000(10.9)	⋯	1000(9.9)	819(−11.0)	825(6.3)	799(−4.1)
$2\nu_9$	1275(2.1)	1122(6.4)	970(1.14)	1139(11.4)	1038(−2.7)	932(4.8)
$\nu_7+\nu_9$	1603(−31.0)	1587(−16.5)	1491(−9.7)	1404(7.0)	1349(0.7)	1276(6.5)
$3\nu_9$	1938(28.6)	1701(−6.1)	1476(7.3)	1694(−8.1)	1577(3.6)	1402(−2.4)
$2\nu_7$	2002(8.3)	2123(9.1)	1997(−0.3)	1661(−8.8)	1635(−1.2)	1592(0.6)
$\nu_7+2\nu_9$	2262(−16.9)	2156(6.4)	2017(−4.6)	1989(17.9)	1887(0.9)	1741(−3.8)
$4\nu_9$	2520(−25.8)	⋯	1975(−3.9)	2267(−16.6)	2112(−2.1)	1890(−0.4)
$2\nu_7+\nu_9$	2656(9.0)	⋯	⋯	⋯	2171(−8.2)	2067(2.0)
$\nu_7+3\nu_9$	2956(32.1)	⋯	⋯	2552(0.3)	2433(0.9)	2229(−0.2)
$3\nu_7$	3012(−1.8)	3099(−3.0)	3020(−1.5)	2528(8.6)	⋯	⋯
$2\nu_7+2\nu_9$	3288(−12.4)	⋯	3096(4.7)	⋯	2731(0.6)	2544(−3.6)
$5\nu_9$	⋯	⋯	⋯	2888(15.8)	⋯	⋯
$3\nu_7+\nu_9$	⋯	⋯	⋯	⋯	3012(2.9)	⋯
$\nu_7+4\nu_9$	⋯	3310(0.9)	⋯	3130(−10.5)	⋯	2724(1.4)
$2\nu_7+3\nu_9$	⋯	⋯	⋯	⋯	⋯	3040(0.9)
$\nu_7+5\nu_9$	⋯	⋯	⋯	⋯	⋯	3225(0.2)
$4\nu_7$	⋯	⋯	⋯	3376(−2.8)	⋯	⋯

shift of ν_7 upon deuteration of the methyl moieties ($CH_3 \rightarrow CD_3$) is calculated to be 21.1%, 21.5%, and 22.1% for CH_3NH_2, CH_3NHD, and CH_3ND_2, respectively, which is in good agreement with the respective experimental values of 16.1%, 24.2%, and 18.9%. Accordingly, all observed vibrational bands could be nicely assigned to the fundamentals, overtones, or combinations of the methyl rocking (ν_7) and amino wagging (ν_9) modes.

Considering anharmonic couplings associated with ν_7 and ν_9 modes, it is then possible to extract at least three anharmonicity constants from the fit using the following equation.[20]

$$G_0(\upsilon_7,\upsilon_9)=\omega_7^0\upsilon_7+\omega_9^0\upsilon_9+x_{77}^0(\upsilon_7)^2+x_{79}^2\upsilon_7\upsilon_9+x_{99}^0(\upsilon_9)^2, \quad (4)$$

where υ_7 and υ_9 are the vibrational quantum numbers for ν_7 and ν_9, respectively, and G_0 represents the term values of

TABLE IV. *Ab initio* vibrational frequencies (cm^{-1}) of methylamines in the $\tilde{A}$ states. The torsional mode (ν_{15}) was not included. The symmetry species (A',A'') is classified according to the MS group of Cs where the molecular plane containing a C–H bond bisects the HNH angle. The symmetry consideration for the torsional mode in the CNPI group of G_{12} has been given in Ref. 17.

Vibration No.	CH_3NH_2	CH_3NHD	CH_3ND_2	CD_3NH_2	CD_3NHD	CD_3ND_2
A'						
ν_1	3419	2514	2475	3416	2514	2475
ν_2	3235	3232	3232	2365	2364	2364
ν_3	2995	3039	3039	2202	2202	2202
ν_4	1646	1498	1246	1640	1486	1251
ν_5	1572	1592	1591	1193	1069	1180
ν_6	1494	1467	1469	1071	1192	1068
ν_7	1145	1129	1109	803	795	778
ν_7 (Expt.)	989	1080	990	830	819	803
ν_8	1049	917	879	983	967	941
ν_9	623	542	460	591	531	454
ν_9 (Expt.)	636	546	479	560	516	459
A''						
ν_{10}	3444	3427	2552	3437	3427	2552
ν_{11}	3317	3275	3276	2436	2435	2435
ν_{12}	1523	1647	1632	1166	1223	1219
ν_{13}	926	800	748	804	720	676
ν_{14}	1308	1333	1330	1263	1109	1082

TABLE V. Harmonic frequencies and anharmonicity constants obtained from fitting the vibrational term values (cm^{-1}) in Table III to Eq. (4).

	CH_3NH_2	CH_3NHD	CH_3ND_2	CD_3NH_2	CD_3NHD	CD_3ND_2
ω_7^0	981.4±22.3	1102.8±16.7	981.6±7.0	825.1±9.4	819.2±3.5	810.6±3.9
ω_9^0	636.4±15.7	535.3±7.6	474.1±5.1	556.7±6.5	512.2±2.9	454.6±1.5
x_{77}^0	7.7±8.5	−22.9±6.2	8.5±2.7	4.9±2.8	−0.6±1.3	−7.4±2.0
x_{99}^0	0.006±4.5	11.2±2.7	5.1±1.5	3.5±1.5	4.1±0.9	4.5±0.4
x_{79}^0	8.5±7.2	−22.9±6.6	31.3±2.5	6.7±3.8	13.3±1.4	7.2±0.8

various quantum states with respect to the zero-point level. Measured experimental values are fitted to Eq. (4) to give the harmonic frequencies and anharmonicity constants associated with ν_7 and ν_9 modes. The fitted values are summarized in Table V, while the differences between the experiment and calculation are listed in Table III. There are large uncertainties for harmonic frequencies and anharmonic constants of CH_3NH_2 and CH_3NHD, and this should be attributed to less accurately measured band positions due to both the intrinsic broad linewidth and severe overlaps of corresponding vibronic bands.[17,18] On the other hand, both harmonic frequencies and anharmonic constants are quite precisely determined for some isotopomers such as CD_3ND_2 and CD_3NHD. The x_{79}^0 constant is quite large for CH_3NHD and CH_3ND_2 for which the frequency of ν_7 is relatively close to twice that of ν_9, indicating that the small energy difference between ν_7 and $2\nu_9$ may be responsible for the larger coupling matrix element. It should be noted, however, that Eq. (4) excludes any coupling to optically dark states and large uncertainties of anharmonicity constants obtained for some isotopomers in Table V could be indicative of the existence of such couplings.

C. The torsional barrier height depending on the vibrational excitation

One of the interesting experimental findings is that the torsional barrier height increases when the amino wagging mode (ν_9) is excited. That is, the torsional barrier height, which is 5 or 5.5 cm^{-1} at the zero-point energy level, increases to 19 cm^{-1} with ν_9 mode excitation for CH_3ND_2 (Refs. 17 and 18) or CD_3ND_2. The mode dependence of the torsional barrier height of methylamine is especially intriguing when this is compared with that found for the CH_3CH_2 radical in the ground state. Sears *et al.*[21] and Johnson and Sears[22] found that the torsional barrier of $CH_3CH_2(X)$ in the zero level is 17 cm^{-1} and it decreases to 10 cm^{-1} when one quantum of the CH_2 rocking mode is excited, which is the opposite trend to the case of $CH_3NH_2(\tilde{A})$. The $CH_3CH_2(X)$ radical is isoelectronic to the CH_3NH_2 cation: the electronic structure of those two species should be similar. Accordingly, the electronic energy associated with the torsional motion is expected to be quite similar for $CH_3CH_2(X)$ and $CH_3NH_2(\tilde{A})$. However, as pointed out earlier by Sears *et al.*[21] and Johnson and Sears,[22] when the torsional barrier height is small the change of the vibrational energy as a function of the torsional angle becomes the dominant factor in determining the effective torsional barrier height. Therefore, the explanation for the different mode dependence of the torsional barrier of $CH_3CH_2(X)$ and $CH_3NH_2(\tilde{A})$ should originate from the difference in the vibrational energy changes of two molecules with the change of the torsional angle.

Since the torsional motion is much slower compared to the other vibrational motions, it is reasonable to calculate the effective torsional barrier height based on the following equation, introduced by Johnson and Sears:[22]

$$V(\phi) = E_{\mathrm{el}}(\phi) + \sum_n h\omega_n(\phi)(v_n + 1/2). \tag{5}$$

Here $E_{\mathrm{el}}(\phi)$ is the electronic energy as a function of torsional angle, while $\omega_n(\phi)$ and v_n are the vibrational frequency and number of quanta of the nth mode, respectively. The sum is over all vibrational modes except the torsional mode. For the CH_3CH_2 radical, it was reported in Ref. 22 that the torsional barrier is 17.6 cm^{-1} in the zero level and 10.9 cm^{-1} for the $v=1$ level of the CH_2 rocking mode. This calculation was carried out by using the B3LYP method with the basis set of 6-311++G$(2df,2pd)$, and it reproduces the experimental result well.[22] Here, we calculate the barrier height of $CH_3NH_2(\tilde{A})$ by the same way using Eq. (5) using the configuration interaction singles (CIS) method with the 6-311++G$(2df,2pd)$ basis set. In Fig. 4, the calculated torsional barriers at the zero-point level, with one quantum of the NH_2 wag (ν_9), and the level with one quantum of the CH_3 rock (ν_7) are plotted as a function of the torsional angle. In the calculation, all degrees of freedom are relaxed except the

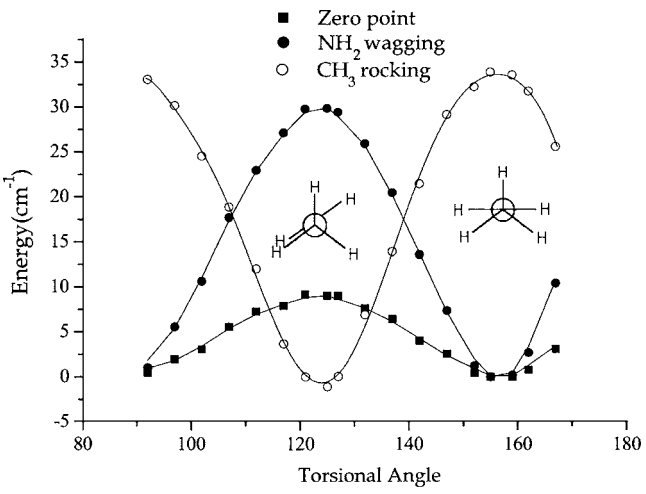

FIG. 4. The calculated torsional potential energy curves in the zero-point energy level (■), with the NH_2 wagging mode (ν_9) excitation (●), or with CH_3 rocking mode (ν_7) excitation (○) plotted vs the torsional angle around the C–N axis. The calculation was carried out by using the CIS method with the 6-311++G $(2df,2pd)$ basis set.

TABLE VI. The torsional barrier height (cm^{-1}) calculated for the excited, ground, and cationic states of CH_3NH_2.

Calc. (method/basis set)	Zero level	$v=1$ of NH_2 wag	$v=1$ of CH_3 rock
Excited state CIS/6-311++G(2*df*,2*pd*)	9.2	29.8	−33.9[a]
Cationic state B3LYP/6-311++G(2*df*,2*pd*)	9.0	19.5	−11.5[a]
Ground state B3LYP/6-311+G(*d*,*p*)	688.0[b]	652.0	684.0

[a]The negative value of the barrier height indicates that the eclipsed from of CH_3NH_2 becomes the minimum energy structure. The torsional potential curve becomes upsidedown compared to that at the zero-point level.
[b]The experimental value is 690 cm^{-1} (Ref. 23).

fixed torsional angle to give the minimum energy and associated vibrational frequencies. The barrier height from the calculation is then found to be 9.2 cm^{-1} for the zero-point level, while it is 29.8 cm^{-1} for the level with one quantum of NH_2 wag (ν_9) (Fig. 4). Even though the theoretical value does not reproduce the experiment perfectly in terms of the absolute value, the calculation still seems to be in good agreement with the experiment. Moreover, it is quite remarkable that the experimental trend of the torsional barrier with ν_9 excitation is so well explained by the calculation. The other interesting theoretical finding is that the torsional barrier height is calculated to be 33.9 cm^{-1} and the minimum energy structure is changed to the eclipsed form when the CH_3 rocking mode (ν_7) is excited by one quantum (Fig. 4). This torsional potential for the ν_7 ($v=1$) level which is upsidedown compared to the that at the zero point or ν_9 ($v=1$) level could be responsible for the shape of the ν_7 rovibrational band which is quite different from that of ν_9, as clearly shown in Figs. 1 and 3. The dramatic change of the torsional potential upon vibrational excitation indicates that the torsional barrier height, especially when it is small, may be truly dominated by the vibrational energy of modes which are perpendicular to the torsional angle. At high internal energies where mode couplings are expected to be active, a more complicated expression for the barrier potential would be needed.

We have also carried out the same calculations for the cationic and ground neutral states of CH_3NH_2 (Table VI). In the cationic ground state of CH_3NH_2, the torsional barrier height is found to be 9.0, 19.5, and −11.5 cm^{-1} for the zero level, $v=1$ of the ν_9^+ mode, and $v=1$ level of the ν_7^+ mode, respectively, when it is calculated by using the B3LYP method using the 6-311++G(2*df*,2*pd*) basis set. The negative sign of the torsional barrier height indicates that the torsional potential becomes upsidedown at the level with the ν_7^+ mode excited, as in the case of $CH_3NH_2(\tilde{A})$. This calculation is consistent with the experimental observation that the torsional barrier becomes higher when one quantum of the NH_2 wagging mode is combined with the torsional mode.[16,17] Meanwhile, the torsional barrier for CH_3NH_2 in the ground electronic state is calculated to be quite high, giving the value of $V_6=688.0$ cm^{-1}. Amazingly, this is in excellent agreement with the experimental value of 690 cm^{-1} for $CH_3NH_2(X)$.[23] For ground state CH_3NH_2, the torsional barrier is quite high, the effect of vibrational energy on the barrier height is found to be less significant, giving $V_6=652$ or 684 cm^{-1} for the level with the ν_9 or ν_7 mode excitation, respectively (Table VI). It is interesting to note that the NH_2 wagging mode excitation in $CH_3NH_2(X)$ lowers the torsional barrier; this is in the opposite trend to the case of the excited or cationic state.

IV. CONCLUSIONS

Here, the spectroscopic characterization of six methylamine isotopomers (CH_3NH_2, CH_3NHD, CH_3ND_2, CD_3NH_2, CD_3NHD, and CD_3ND_2) in the first electronically excited state has been carried out. The internal/overall rotation Hamiltonian is used for the spectral analyses for all observed rovibronic bands to give accurate vibrational band positions, associated rotational constants, rotational temperature, and predissociation lifetimes. Vibrational frequencies and anharmonicity constants associated with amino wagging (ν_9) and methylrocking (ν_7) modes are precisely determined to give the detailed shape of the potential energy surface along the corresponding nuclear motions. The torsional barrier height is found to be strongly dependent on vibrational excitation, and its increase with ν_9 excitation is theoretically well explained for $CH_3NH_2(\tilde{A})$. In fact, the torsional barrier height seems to originate from vibrational energy as a function of torsional angle when the electronic origin for the torsional barrier is less important. In conclusion, the long-time confusion about the origin positions, vibrational assignments, and rotational structures of various methylamine isotopomers in the $\tilde{A}$ state is completely resolved. Dynamical studies of methylamines based on this firm spectroscopic framework will be investigated in the near future.

ACKNOWLEDGMENT

This work was financially supported by Korea Research Foundation (KRF-2005-070-C00063).

[1] T. Föster and J. C. Jurgens, Z. Phys. Chem. Abt. B **36**, 387 (1937).
[2] E. Tannenbaum, E. M. Coffin, and A. J. Harrison, J. Chem. Phys. **21**, 311 (1953).
[3] J. V. Michael and W. A. Noyes, J. Am. Chem. Soc. **85**, 1228 (1963).
[4] M. Tsuboi, A. Y. Hirakawa, and H. Kawashima, J. Mol. Spectrosc. **29**, 216 (1969).
[5] M. Tsuboi and A. Y. Hirakawa, Can. J. Phys. **60**, 844 (1982).
[6] H. K. Haak and F. Stuhl, J. Phys. Chem. **88**, 3627 (1984).

[7] E. P. Gardner and J. R. McNesby, J. Phys. Chem. **86**, 2646 (1982).
[8] T.-X. Xiang and W. A. Guillory, J. Chem. Phys. **85**, 2019 (1986).
[9] G. C. G. Waschewsky, D. C. Kitchen, P. W. Browning, and L. J. Butler, J. Phys. Chem. **99**, 2635 (1995).
[10] D. P. Taylor and E. R. Bernstein, J. Chem. Phys. **103**, 10453 (1995).
[11] D. P. Taylor, C. F. Dion, and E. R. Bernstein, J. Chem. Phys. **106**, 3512 (1997).
[12] C. L. Reed, M. Kono, and M. N. R. Ashfold, J. Chem. Soc., Faraday Trans. **92**, 4897 (1996).
[13] M. N. R. Ashfold, R. N. Dixon, M. Kono, D. H. Mordaunt, and C. L. Reed, Philos. Trans. R. Soc. London, Ser. A **355**, 1659 (1997).
[14] K. M. Dunn and K. Morokuma, J. Phys. Chem. **100**, 123 (1996).
[15] M.-J. Hubin-Franskin, J. Delwiche, A. Giuliani, M.-P. Ska, F. Motte-Tollet, I. C. Walker, N. J. Mason, J. M. Gingell, and N. C. Jones, J. Chem. Phys. **116**, 9261 (2002).
[16] S. J. Baek, K.-W. Choi, Y. S. Choi, and S. K. Kim, J. Chem. Phys. **118**, 11040 (2003).
[17] S. J. Baek, K.-W. Choi, Y. S. Choi, and S. K. Kim, J. Chem. Phys. **118**, 11026 (2003).
[18] S. J. Baek, K.-W. Choi, Y. S. Choi, and S. K. Kim, J. Chem. Phys. **117**, 10057 (2002).
[19] M. J. Frisch, G. W. Trucks, H. B. Schlegel *et al.*, GAUSSIAN 03W, Gaussian, Inc., Pittsburgh, PA, 2003.
[20] G. Herzberg, *Electronic Spectra of Polyatomic Molecules* (Van Nostrand Reinhold, New York, 1966).
[21] T. J. Sears, P. M. Johnson, and J. BeeBe-Wang, J. Chem. Phys. **111**, 9213 (1999).
[22] P. M. Johnson and T. J. Sears, J. Chem. Phys. **111**, 9222 (1999).
[23] D. Kivelson and D. R. Lide, Jr., J. Chem. Phys. **27**, 353 (1957).